Supplementary Information (SI) for Materials Advances.
This journal is © The Royal Society of Chemistry 2026

Electronic Supporting Information

Unveiling reline deep eutectic solvent (DES) for controlled synthesis of phase-pure $CuFeS_2$ towards dielectric and electrocatalytic applications

Bhagirath Mahto, Monika Gupta, Haider Ali and Sahid Hussain*

***Corresponding Author**
Department of Chemistry, Indian Institute of Technology Patna, Bihta, 801106, India
Email: sahid@iitp.ac.in; Phone: +91-6115-233022

General Remarks on Safety Concerns During Synthesis

The synthesis of $CuFeS_2$ in a sealed autoclave using reline DES as the solvent, along with sulfur precursors such as thiourea (TU), thioacetamide (TAA), and sodium sulfide (Na_2S), leads to the buildup of volatile and toxic H_2S gas inside the autoclave. These volatile, toxic sulfur compounds are released when the autoclave is opened. Similarly, when synthesis is performed in thio-reline DES, a highly intense foul odor is released after the sealed autoclave is opened.

Caution! *Preventive measures are required from direct exposure to volatile and toxic H_2S gas; all post-synthetic steps, including washings/cleaning of autoclaves, should be conducted in a well-functioning fume hood with proper containment and ventilation measures. Leftover solutions must be treated with an appropriate oxidizing agent ($KMnO_4$ solution) to neutralize the odor through oxidation.*

Characterizations:

Attenuated Total Reflectance-Fourier Transform Infrared (ATR-FTIR) Spectroscopy

A Perkin Elmer spectrum 400 FT-IR (Fourier transform infrared) spectrophotometer (United States) was used for FTIR measurements of choline chloride (ChCl), urea, and ChCl/U DES (1:2, reline) in the attenuated total reflectance (ATR) mode in the wavenumber range of 4000–600 cm^{-1}.

Nuclear Magnetic Resonance Spectroscopy

Proton nuclear magnetic resonance (^{1}H NMR) spectra of the ChCl, urea and ChCl/U DES were recorded on Bruker 400 MHz spectrometers, using DMSO-d_6 as an NMR solvent. Spectra were processed by using MestReNova. Spectra taken in DMSO-d_6 were referenced to the solvent (DMSO-d_6 = 2.5 ppm) as an internal standard.

Powder X-ray Diffraction

Powder X-ray diffraction (P-XRD) data were recorded in the 2θ range of 10–70° on a PANalytical X-ray diffractometer with Cu Kα (λ = 1.5406 Å) radiation (45 kV, 40 mA). Data were collected in the reflection mode with a step size of 0.02°. Samples were placed on zero background holders made from 32 mm diameter silicon single crystal substrates. One side of the substrate is flat while the other side has a recess of 15 mm diameter x 0.2 mm deep. PANalytical HighScore Plus XRD analysis software was used to process the P-XRD patterns and then the peaks were compared to the reference powder diffraction files (PDFs) from the ICDD (PDF Release 2) and COD database.

Raman Spectroscopy

Raman spectra of the material was recorded at room temperature by a micro Raman spectrometer (STR 750 RAMAN spectrograph, Seki Technotron Corp, Japan) with a laser source of wavelength 633 nm.

Scanning Electron Microscopy

Powdered material was immobilized on a small piece of conductive carbon tape and affixed to a metal stub. Scanning electron microscopy (SEM) of the sample was then carried out at 5 kV with Zeiss Gemini SEM500 instrument in InLens mode.

Transmission Electron Microscopy

Sample for TEM and STEM/EDS mapping was prepared by dispersing the material in ethanol followed by sonication for 30 min. A drop of the solution was placed on the surface of an ultrathin carbon-coated 200 mesh Cu-supported TEM grid (Ted Pella Inc.). The solvent was then allowed to evaporate and dry in air. TEM and high-resolution TEM (HR-TEM) micrographs, selected area electron diffraction (SAED) patterns, and STEM energy dispersive X-ray spectroscopy (EDS) mapping were obtained using a JEOL JEM 200 electron microscope. Gatan microscopy suite software and ImageJ software were used to analyze the TEM images**.**

X-ray Photoelectron Spectroscopy

X-ray photoelectron spectra (XPS) were obtained using a Thermo Fisher Scientific ESCALAB XI^+ X-ray photoelectron spectrometer with a Mg Kα excitation source with binding energy corrected by C 1s (284.8 eV). Wide energy scans ranging from 0 to 1200 eV binding energy were used to identify surface elements, while high-resolution spectra were recorded specifically for Cu 2p, Fe 2p, S 2p, and O 1s.

Thermogravimetric Analysis (TGA)

Thermogravimetric analysis (TGA) was performed on an SDT Q600 instrument with a controlled heating rate of 10 °C/min in an N_2 environment.

Diffuse Reflectance Spectroscopy

Diffuse reflectance spectroscopy (DRS) was carried out with a UV–Vis-NIR spectrophotometer (Shimadzu UV2600) using $BaSO_4$ as a reflectance standard in the 200-1400 nm wavelength range. The reflectance data was converted to Kubelka Munk (K-M) function ($F(R_\infty)$), which is equivalent to the absorption coefficient (α) using the **Equation S1** as shown below:

$$F(R_\infty) = \frac{K}{S} = \frac{(1 - R_\infty)^2}{2R_\infty} \quad \text{(S1)}$$

where $R_\infty = \frac{R_{sample}}{R_{standard}}$ is the reflectance of an infinitely thick specimen, while K and S are K-M scattering and absorption coefficients, respectively. Then, **Equation S2** was used to calculate the band gap values by extrapolation of the linear portion of the $(F(R_\infty) \times h\nu)^{1/n}$ curve versus the photo energy (hν).

$$(h\nu F(R_\infty))^{1/n} = A(h\nu - E_g) \quad \text{(S2)}$$

where E_g is the material's band gap, $h\nu$ is the photon energy in eV, A is a constant, and $F(R_\infty)$ is the Kubelka-Munk coefficient. The n factor depends on the nature of the transition and is equal to the ½ or 2 for the direct and indirect allowed transition band gap, respectively.

Ultraviolet-Visible Spectroscopy

Ultraviolet-visible (UV-Vis) spectrum was recorded using a Shimadzu UV2550 spectrophotometer with 3 ml quartz cuvette with a path length of 1 cm in the 200-800 nm wavelength range.

Gas Adsorption

Brunauer–Emmett–Teller (BET) specific surface area (SSA) and porosity were obtained from an N_2 adsorption-desorption isotherm at 77 K using a Quantachrome Autosorb iQ2 analyzer. Prior to the measurements, the sample was degassed under a vacuum for 6 h at 90 °C. The BET SSA was calculated from the adsorption data in the relative pressure (P/P_0) range from 0.05 to 0.35. Pore

size distribution was estimated using the Barrett–Joyner–Halenda (BJH) method using the desorption branch of N_2 isotherm.

Inductively Coupled Plasma Mass Apectrometry (ICP-MS)

The metal content in the electrolyte after the long-term stability test was quantified using ICP–MS, 7800, Agilent, USA.

Photoresponsive Current-Voltage (I-V) Study

For the photoresponsive current-voltage (I-V) study, the powdered material of $CuFeS_2$ nanocrystals was pressed into a pellet using a hydraulic press. Subsequently, conducting silver paste was applied to make two small point-like probes on the surface. The pellet was then dried at 100 °C for 2 hours to enhance the adhesion of the silver paste. After that, the photo response of $CuFeS_2$ was evaluated by measuring its current-voltage (I-V) behavior using a Keithley 2636A source meter under both dark and illuminated conditions (Tungsten filament lamp) by applying bias potential (DC voltage) of -1V to +1 V under ambient conditions. To keep the temperature stable and avoid heating the sample from the light, it was positioned 10 cm away from the light source during the experiment.

Pre-treatment of Carbon Cloth (CC)

The commercial carbon cloth (1.5 cm × 1 cm) was initially sonicated in acetone for 1 hour. Afterwards, the carbon cloth was rinsed three times with deionized water for thorough cleaning and then dried at 50 °C overnight. Next, the CC was treated with a "piranha solution" (a mixture of 98 % H_2SO_4 and 30 % H_2O_2 in a 75:25 v/v ratio) at room temperature under ultrasonication for 4 h to completely eliminate any organic ligands from its surface. The CC was then cleaned and

sonicated for 10 minutes each in acetone, ethanol, and deionized water to eliminate surface contaminants. The CC was subsequently dried in an oven at 60 °C for later use.

Conversion to RHE scale

$$E_{(RHE)} = E_{(Hg/HgO)} + E^0_{(Hg/HgO)} + 0.0592\ pH \quad (S3)$$

$$pH\ of\ 1\ M\ KOH = 13.8$$

$$E^0_{(Hg/HgO)} = 0.098\ V$$

$$For\ 1M\ KOH,\ E_{(RHE)} = E_{(Hg/HgO)} + 0.098 + 0.059 * 13.8$$

$$= E_{(Hg/HgO)} + 0.098 + 0.8142$$

$$= E_{(Hg/HgO)} + 0.9122$$

Overpotential

The overpotential values for each catalyst were calculated at a reference current density of 10 mA cm^{-2} using the following formula:

$$\eta_{(OER)} = (E_{obs} - 1.23)\ V\ versus\ RHE \quad (S4)$$

Thus, the overpotential value is calculated by subtracting 1.23 V (thermodynamic potential for water oxidation) from the measured potential values (vs RHE).

The Tafel Slope

The Tafel slopes were determined by fitting the overpotential to log (j) plots using the Tafel equation provided below:

$$\eta = a + b \times \log(j) \quad (S5)$$

where "b" represents the Tafel slope, "j" denotes the current density, and "a" is the intercept of the slope, which allows for the calculation of the exchange current density.

Electrochemical Active Surface Area (ECSA)

The electrochemically active surface area (ECSA) is determined from the double-layer capacitance (C_{dl}) values of the catalysts. To assess C_{dl}, the non-Faradaic region of the cyclic voltammogram was selected. Cyclic voltammograms at various scan rates of 20, 40, 60, 80, and 100 mV s^{-1} were recorded for all catalysts in the range of 0.3 to 0.4 V versus Hg/HgO. The half-difference between the anodic and cathodic current densities ($\Delta J=(J_a-J_c)/2$), plotted against the scan rates at the central potential, yields a slope that corresponds to the double-layer capacitance (C_{dl}). The ECSA values for the catalysts were calculated using the formula ECSA = C_{dl}/C_s, where C_s is the capacitance of a flat electrode surface with an area of 1 cm^2, taken as 0.04 mF cm^{-2}.

$$C_{dl}\ (F\ cm^{-2}) = \text{Slope of the plot of } \Delta J/2\ (mA\ cm^{-2}) \text{ vs Scan rate } (mV\ s^{-1}) \quad (S6)$$

$$\text{Geometrical area of the electrode used} = 1 \times 1\ cm^2$$

$$C_{dl}\ (F) = C_{dl}\ (F\ cm^{-2}) \times \text{electrode area}\ (cm^2)$$

$$C_s \text{ of a smooth surface (Ni foam)} = 40\ \mu F\ cm^{-2}$$

$$ECSA\ (cm^2) = C_{dl}\ (F) / C_s\ (F\ cm^{-2})$$

Berthelot's reaction

Berthelot's reaction was employed to detect ammonium ions in the DES reline after heating at both 80 °C and 180 °C. In this process, ammonium ions first react with hypochlorite (OCl^-) to form chloramine (NH_2Cl). The chloramine then reacts with phenol, producing quinone chloramine. This in-situ generated quinone chloramine subsequently reacts with another phenol molecule to form indophenol, leading to a color change in the solution to blue. The absorption spectrum of the solution was measured, with a maximum absorption observed at 640 nm, which corresponds to the indophenol blue.

$$NH_4^+ + OCl^- \rightarrow NH_2Cl + H_2O$$

Chloramine

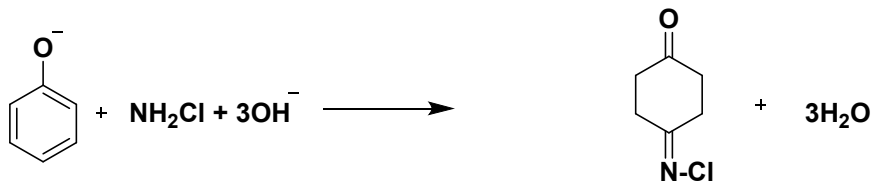

4-(chloroimino)cyclohexan-1-one
(quinonechloramine)

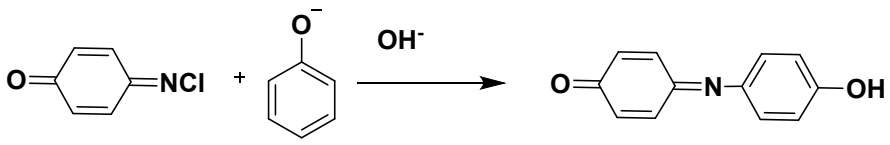

Indophenol

(λ_{max}=640 nm)

Calculation of refractive index

The formula for calculating the refractive index, as provided by Dimitrov and Sakka (**Equation S7**),[1] is expressed as follows:

$$\frac{n^2-1}{n^2-1} = 1 - \sqrt{\frac{E_g}{20}} \tag{S7}$$

where n is the refractive index, and E_g is the direct optical band gap. Likewise, the formula for calculating the refractive index, as proposed by Moss[2] (**Equation S8**), is expressed as follows:

$$n_M = 4\sqrt{\frac{95}{E_g}} \tag{S8}$$

Additionally, the Ravindra model (**Equation S9**) [3]is outlined below, which is reliable across the bandgap range of 1.50 eV < E_g < 3.50 eV, as follows:

$$n_R^2 = 4.084 - [0.62 \times E_g] \tag{S9}$$

According to Herve and Vandamme's model (**Equation S10**),[4], the refractive index is given as follows:

$$n_{HV}^2 = 1 + \left(\frac{A}{E_g + B}\right)^2 \quad \text{(S10)}$$

where A = 13.6 eV, and B = 3.47 eV. This concept is consistent for an energy bandgap range of 2.00 eV< E_g < 4.00 eV. The refractive index from Tripathy model (**Equation S11**) [5] is calculated using the relation:

$$n_T = 1.73 \times [1 + 1.19017 \times e^{-0.539 \times E_g}] \quad \text{(S11)}$$

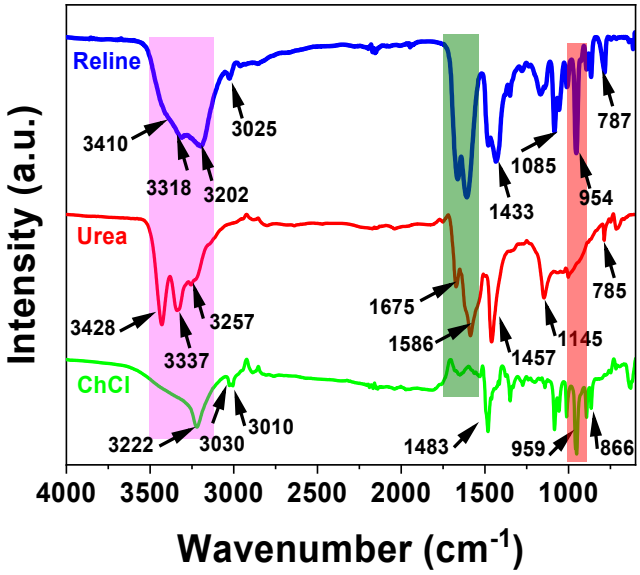

Fig. S1 FTIR spectra of choline chloride (ChCl), urea (U), and choline chloride-urea (ChCl-U) DES.

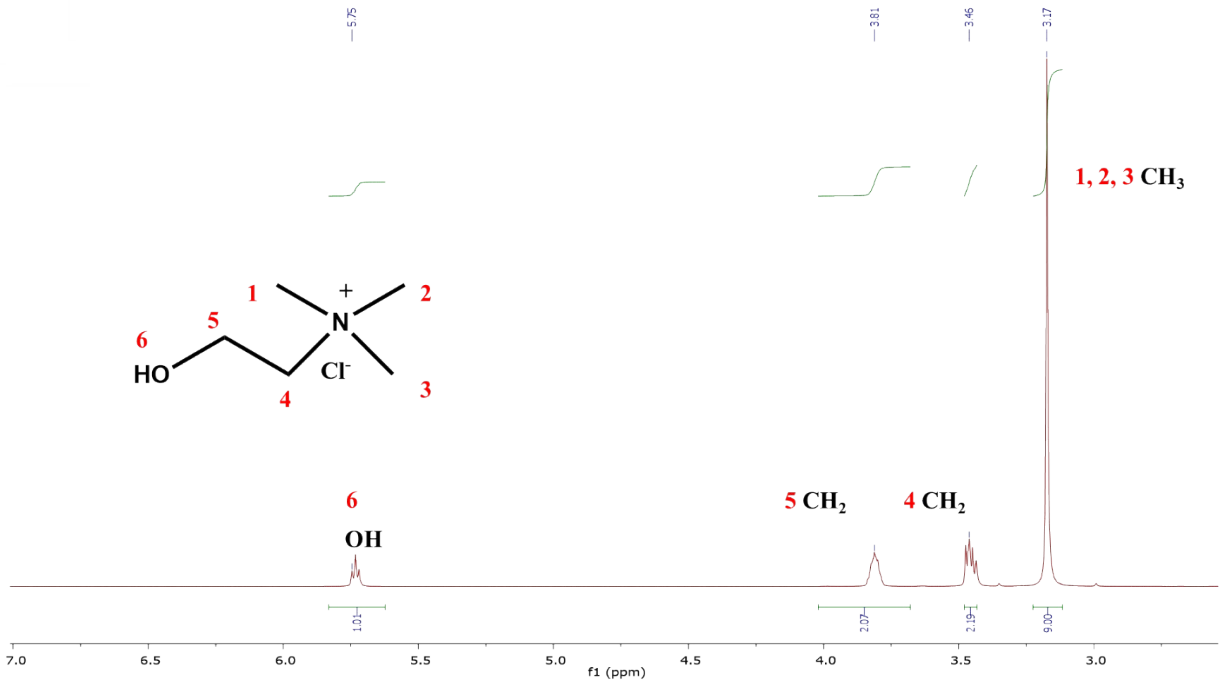

Fig. S2 ^{1}H NMR (400MHz, DMSO-d_6) spectra of choline chloride (ChCl).

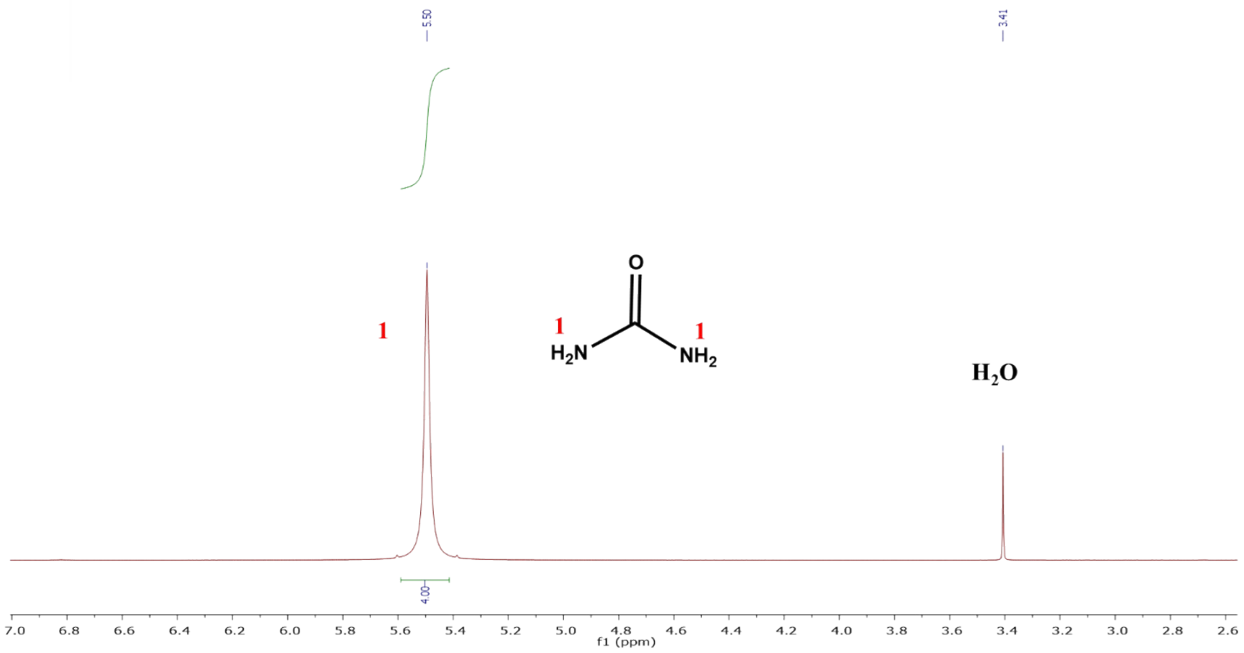

Fig. S3 ^{1}H NMR (400MHz, DMSO-d_6) spectra of urea (U).

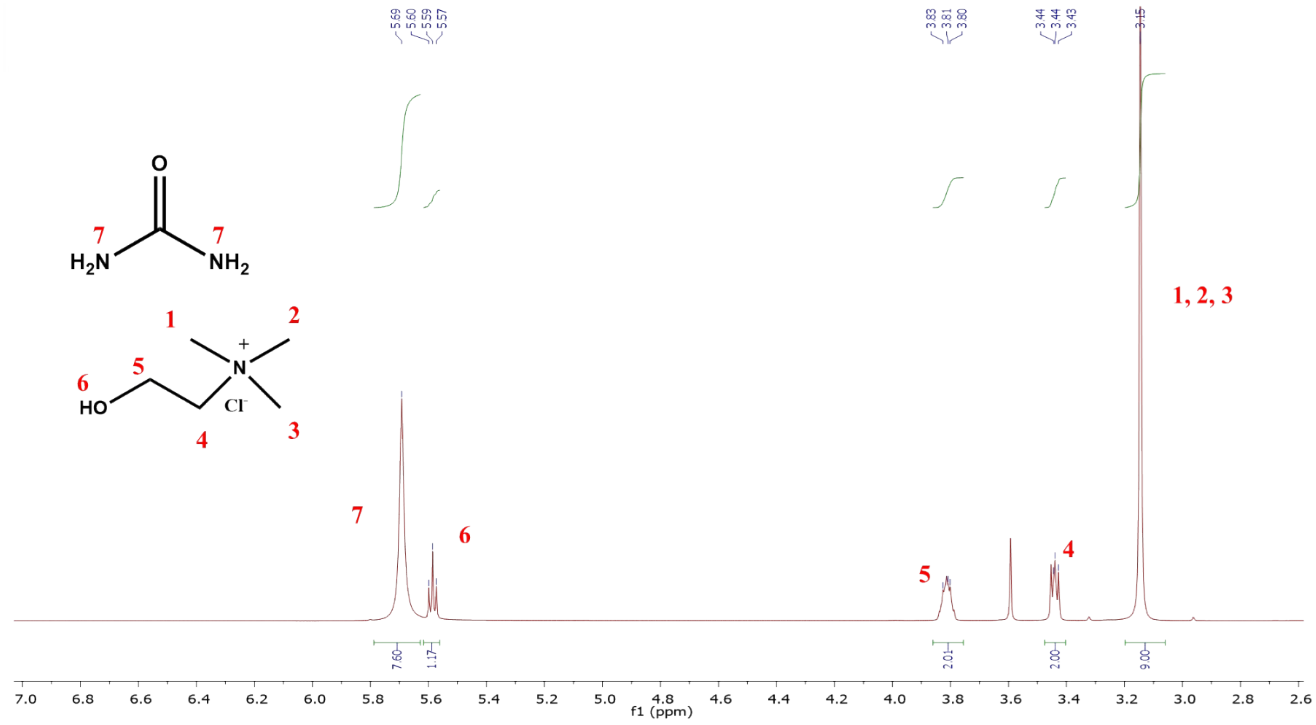

Fig. S4 ^{1}H NMR (400MHz, DMSO-d_6) spectra of ChCl-Urea DES.

Table S1. Chemical Shift and Δδ Values of H Proton of O-H group in ChCl, N-H group in urea, and the ChCl:urea DES.

Components	ChCl	Urea	ChCl-Urea DES	(Δδ)
δ(-OH)/ppm	5.75		5.59	-0.16
δ(-NH)/ppm		5.50	5.69	+0.19

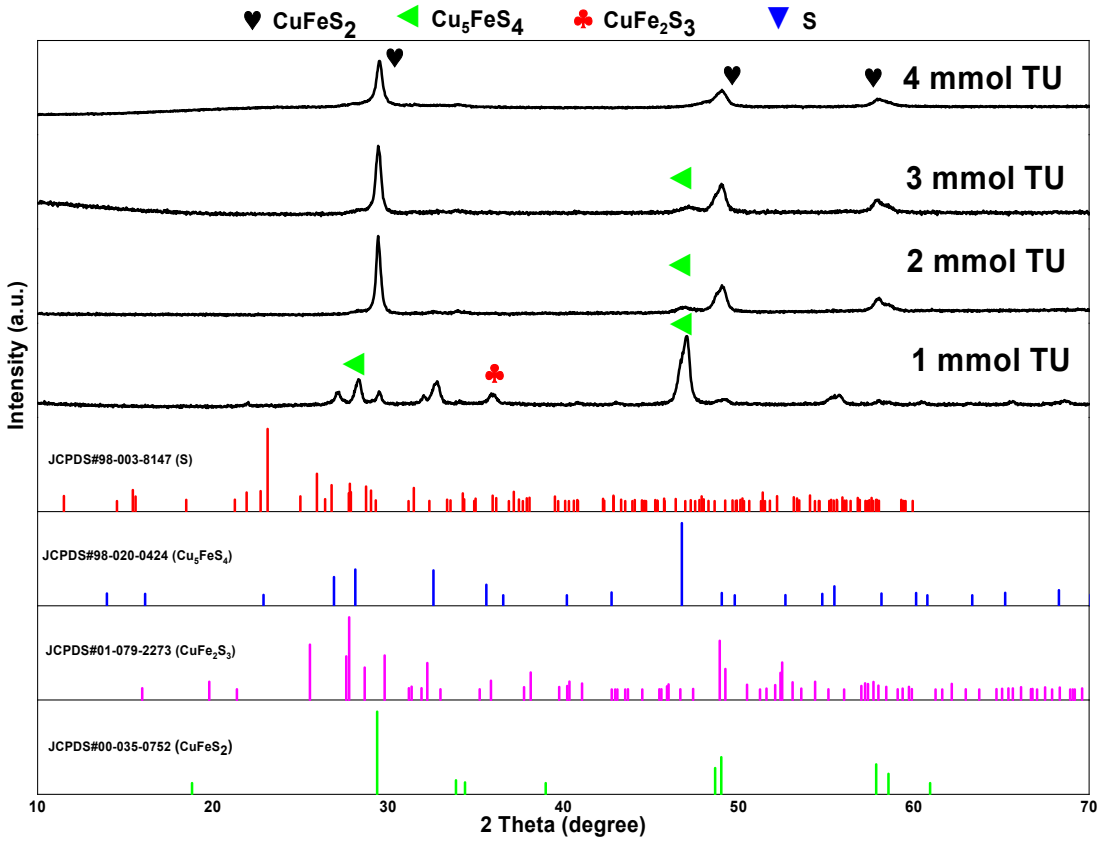

Fig. S5 PXRD patterns of materials synthesized with varying thiourea (1–4 mmol) at a fixed Cu:Fe ratio of 1:1.

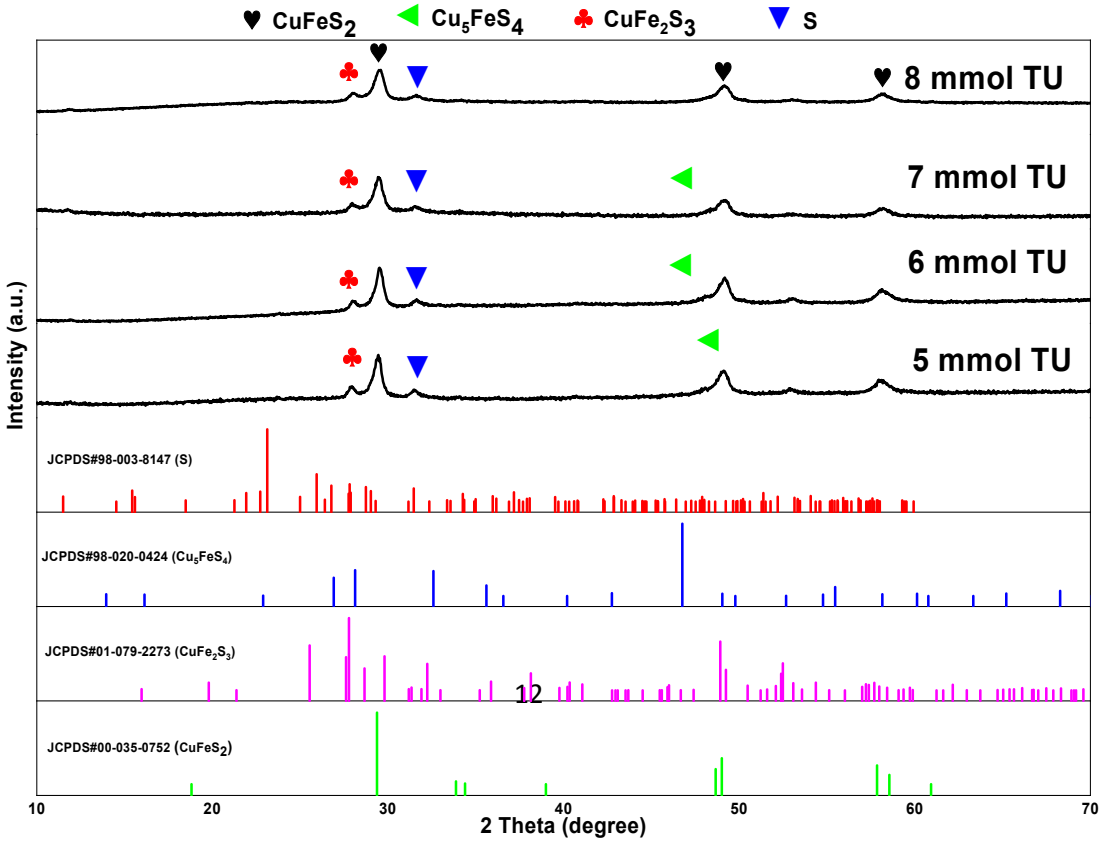

Fig. S6 PXRD patterns of materials synthesized with varying thiourea (5–8 mmol) at a fixed Cu:Fe ratio of 1:1.

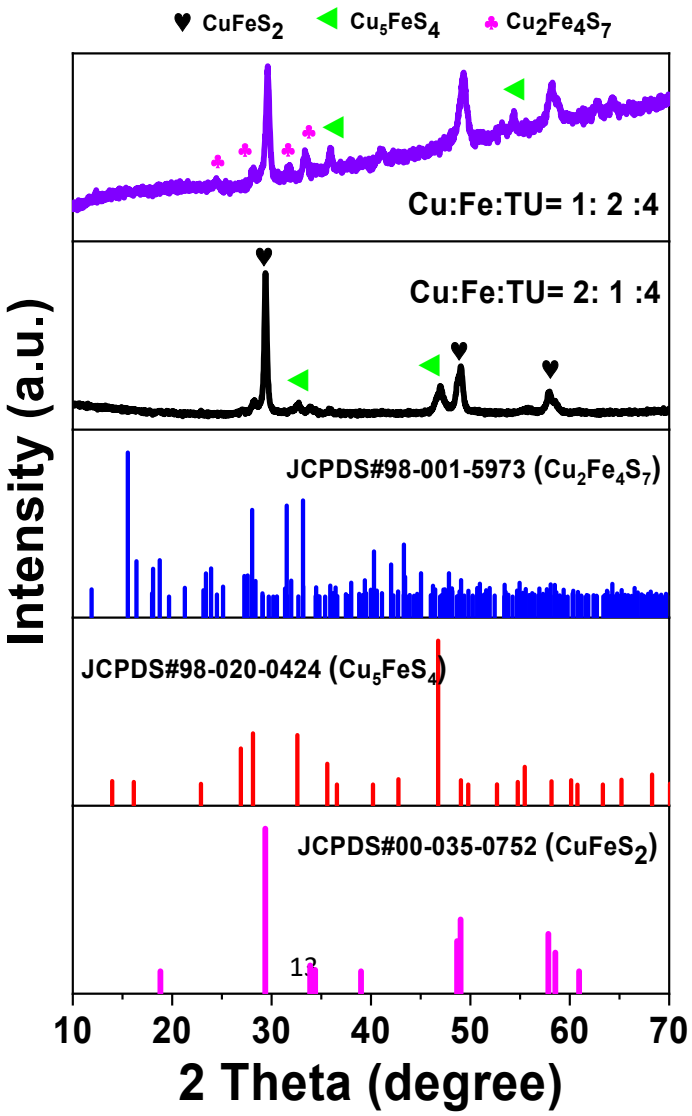

Fig. S7 PXRD patterns of materials synthesized at Cu:Fe ratios of 2:1 and 1:2 with a fixed thiourea concentration of 4 mmol.

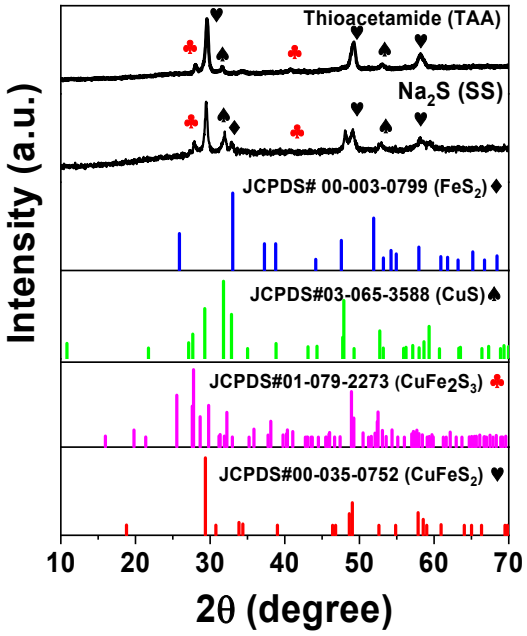

Fig. S8. PXRD pattern of materials synthesized under optimized condition using TAA and SS as sulfur source.

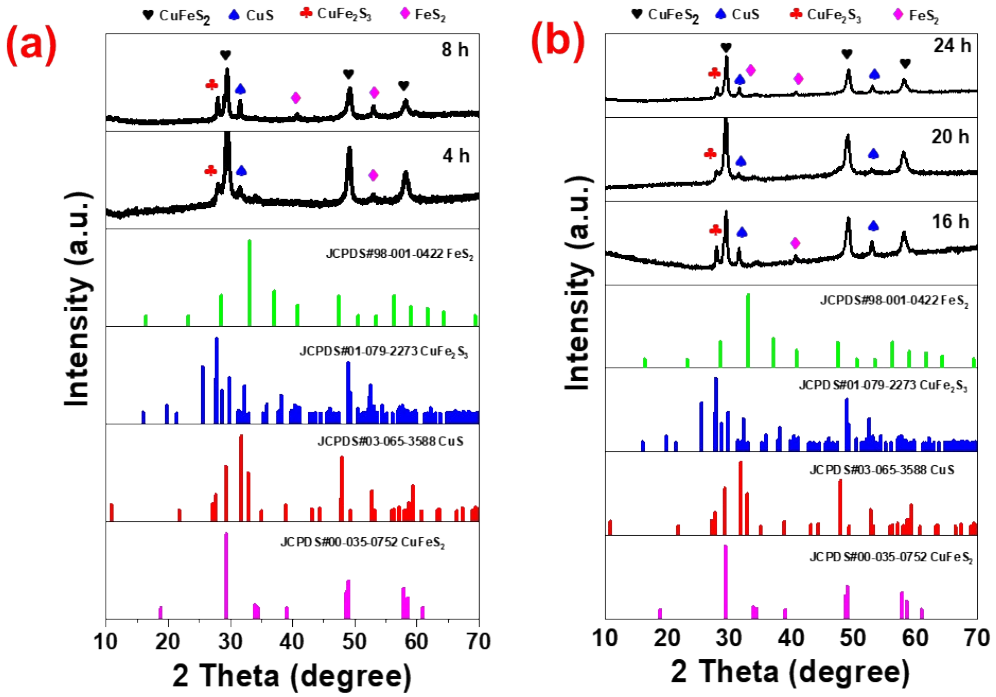

Fig. S9 PXRD patterns of materials synthesized at a Cu:Fe ratio of 1:1 with 4 mmol thioacetamide, varying the reaction time: (a) 4 and 8 h, (b) 16, 20, and 24 h.

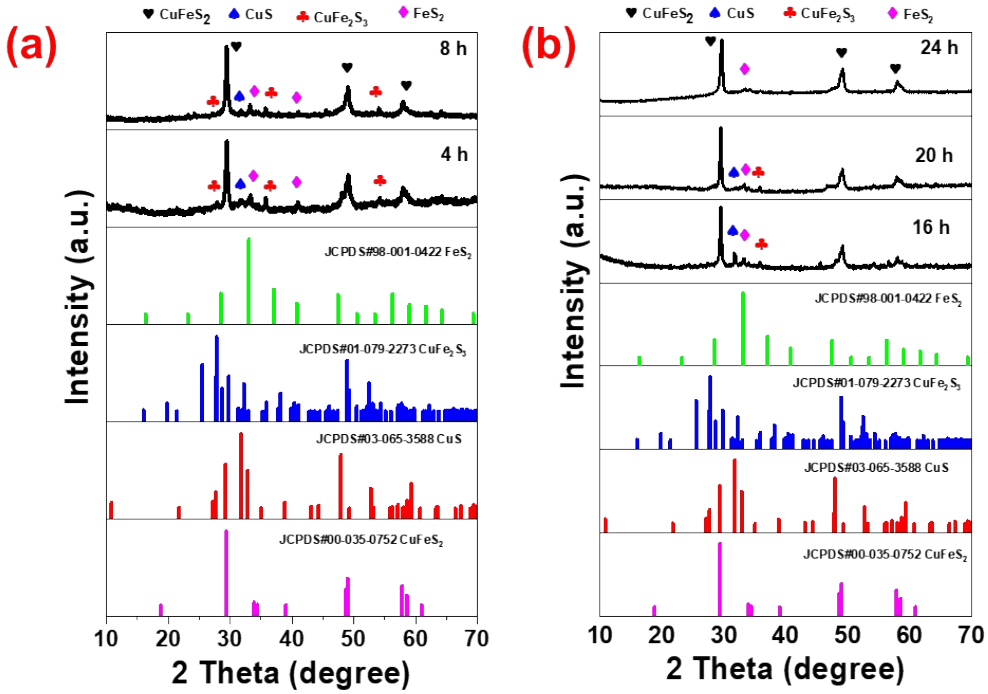

Fig. S10 PXRD patterns of materials synthesized at a Cu:Fe ratio of 1:1 with 4 mmol sodium sulfide, varying the reaction time: (a) 4 and 8 h, (b) 16, 20, and 24 h.

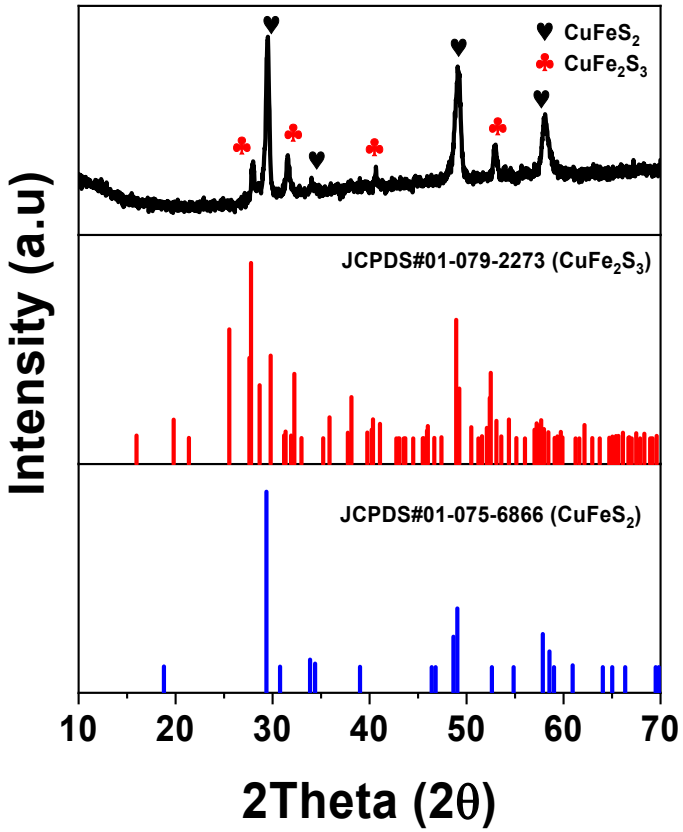

Fig. S11 PXRD patterns for the Cu-Fe-S material synthesized in thio-reline DES under solvothermal conditions of 200 °C for 12 h.

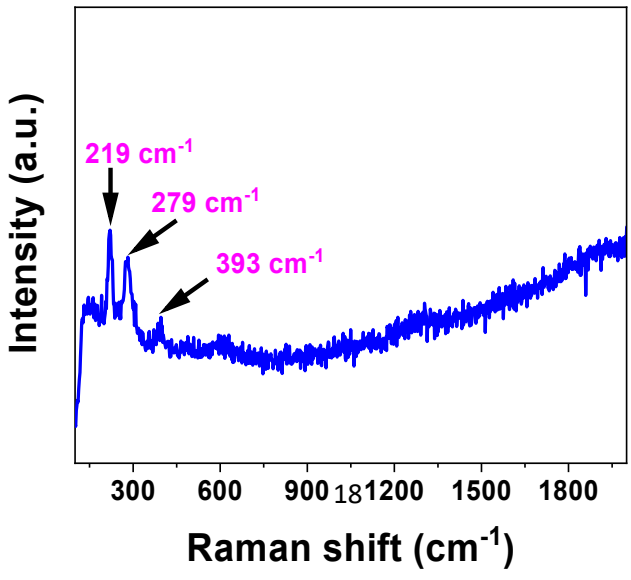

Fig. S12 Raman spectrum of $CuFeS_2$ synthesized in reline DES using thiourea as sulphur precursor.

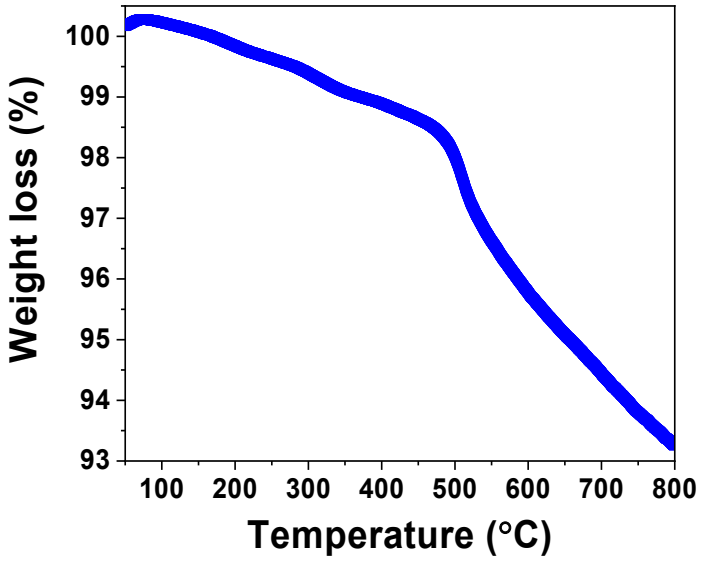

Fig. S13 Thermogravimetric analysis (TGA) of $CuFeS_2$ from ambient to 800 °C in N_2 atmosphere.

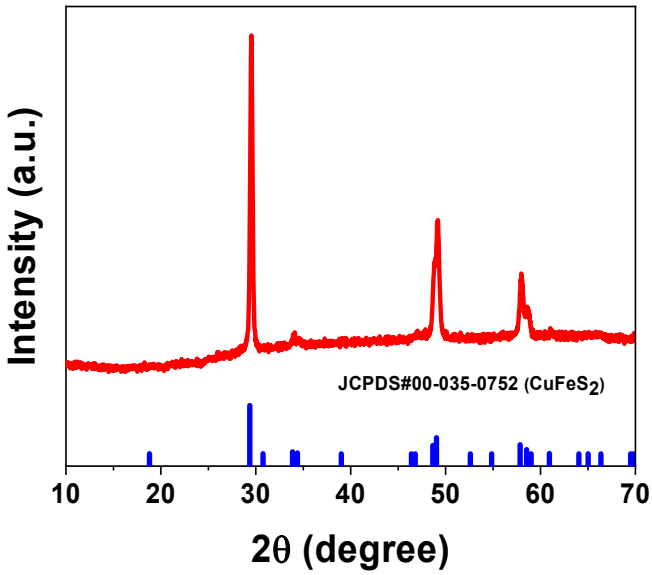

Fig. S14 PXRD pattern of $CuFeS_2$ after thermal treatment in 1-octadecene (ODE).

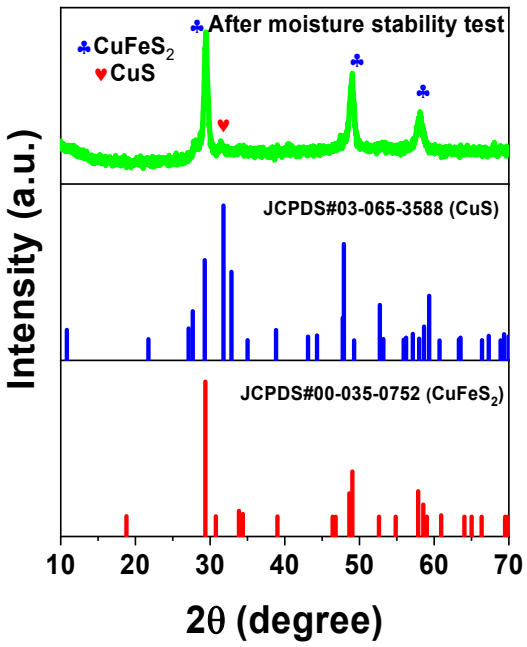

Fig. S15 PXRD pattern of $CuFeS_2$ after exposure to water for 48 h.

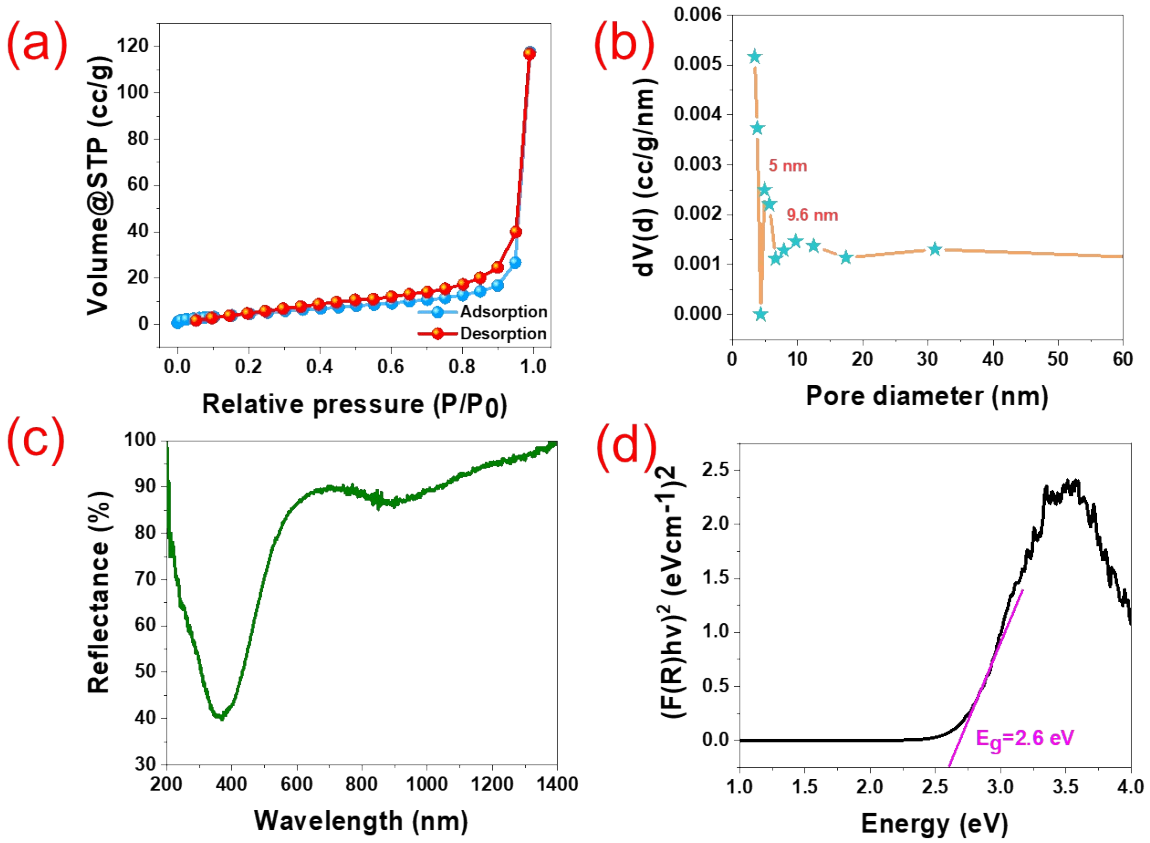

Fig. S16 (a) N_2 adsorption-desorption isotherm, (b) pore-size distribution, (c) diffuse-reflectance spectra (DRS), and (d) Kubelka-Munk plot of $CuFeS_2$.

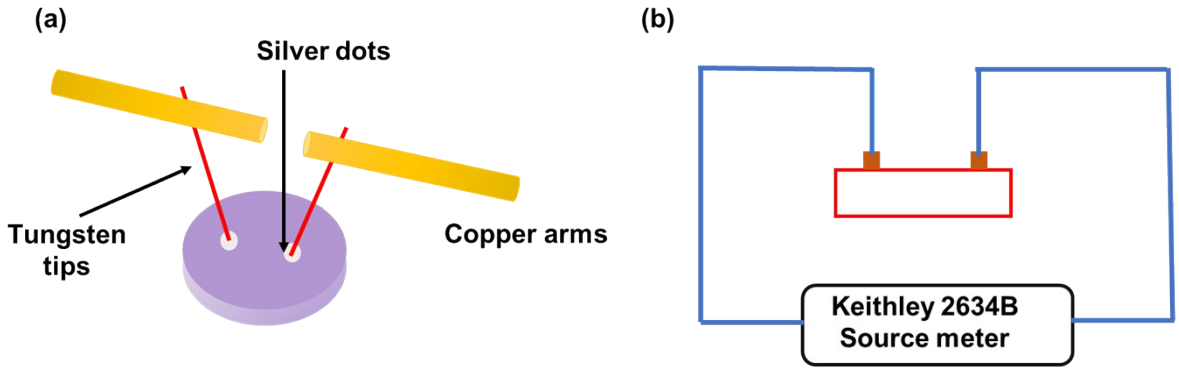

Fig. S17 (a) Schematic drawing of contact of probes with the material, and (b) Schematic illustration for the measurement of I-V.

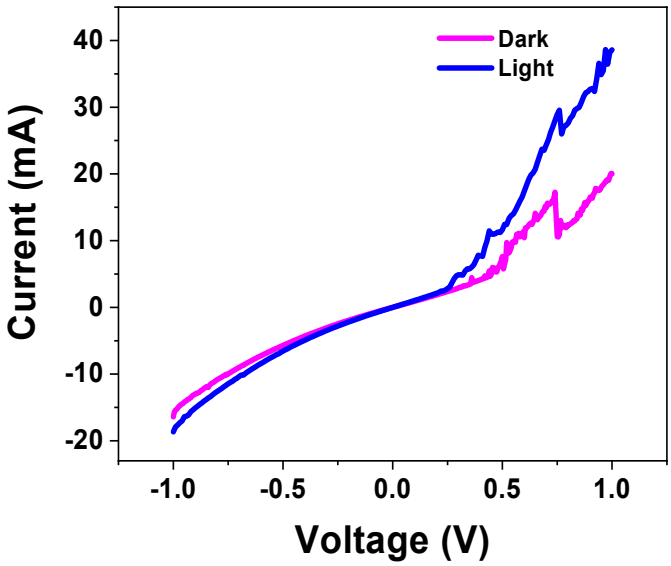

Fig. S18 Current-voltage (I-V) curve of $CuFeS_2$ in dark and light conditions.

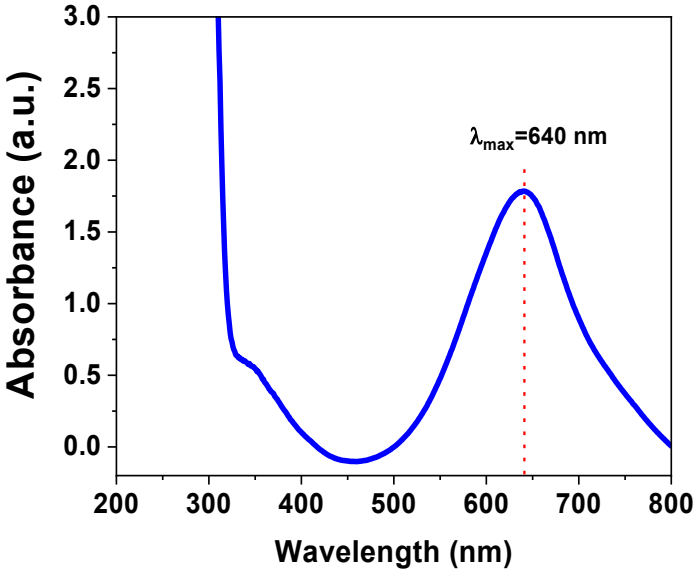

Fig. S19. Absorbance spectra of indophenol formed as a result of Berthelot's reaction with ammonium ions in pure reline.

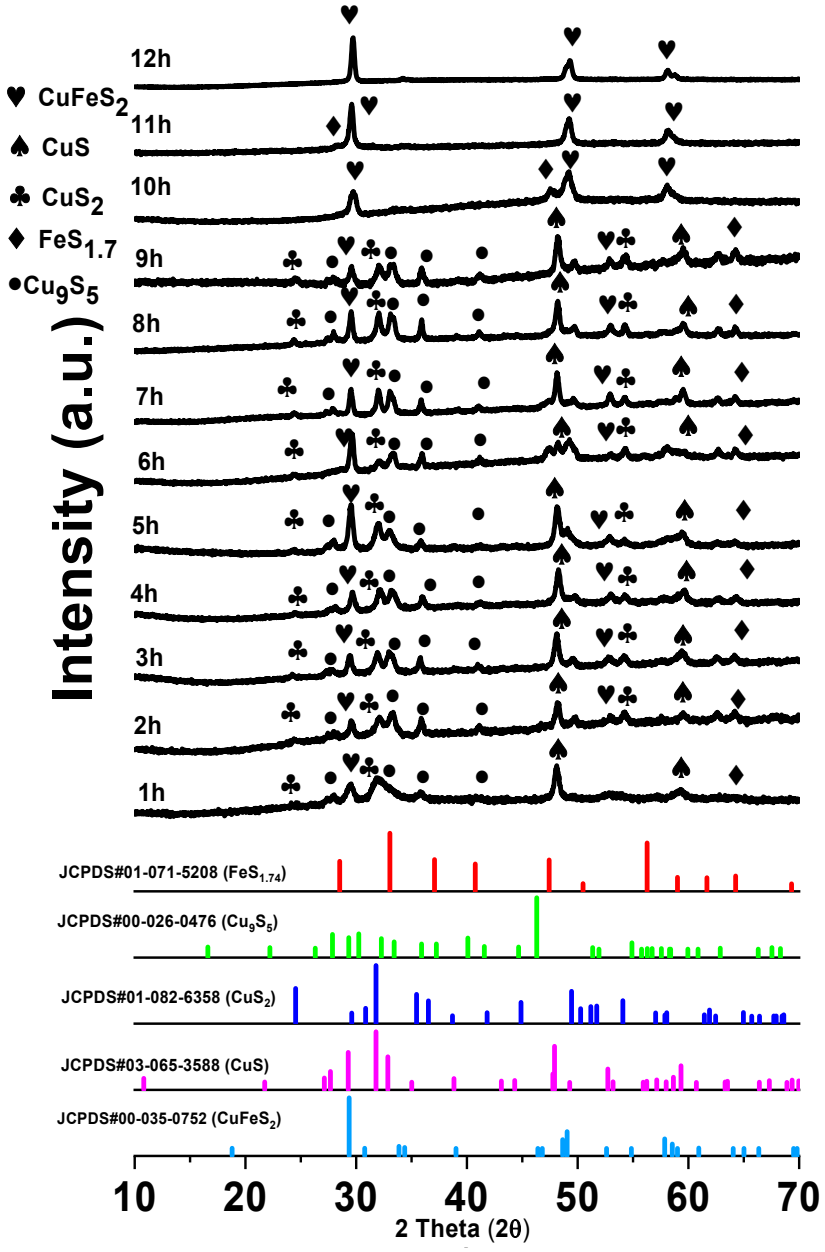

Fig. S20 Time dependent ex-situ PXRD patterns for the phase evolution of $CuFeS_2$ under solvothermal conditions.

Table S2. Visual Observation of reline DES by heating under solvothermal conditions at different time intervals.

Time	Post-heat (200 °C)		Appearance	
	Particulates	**Physical state (liquid, phase separation)**		
1h	None	Liquid, homogeneous	colourless	
3h	None	Liquid, homogeneous	colourless	
6h	None	Liquid, homogeneous	Faint yellow	
9h	None	Liquid, homogeneous	yellow	
12h	None	Liquid, homogeneous	yellow	

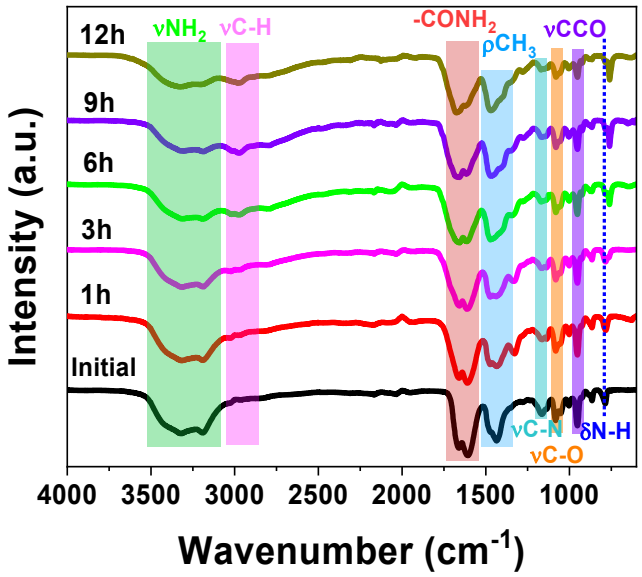

Fig. S21 FTIR of reline DES after heating for different intervals of time.

Table S3: Refractive index of $CuFeS_2$ estimated using different models.

Material	**E_g (eV)**	**$n_{[DS]}$**	**n_M**	**n_R**	**$n_{[HV]}$**	**n_T**
$CuFeS_2$	2.6	2.13	2.46	2.47	2.45	2.54

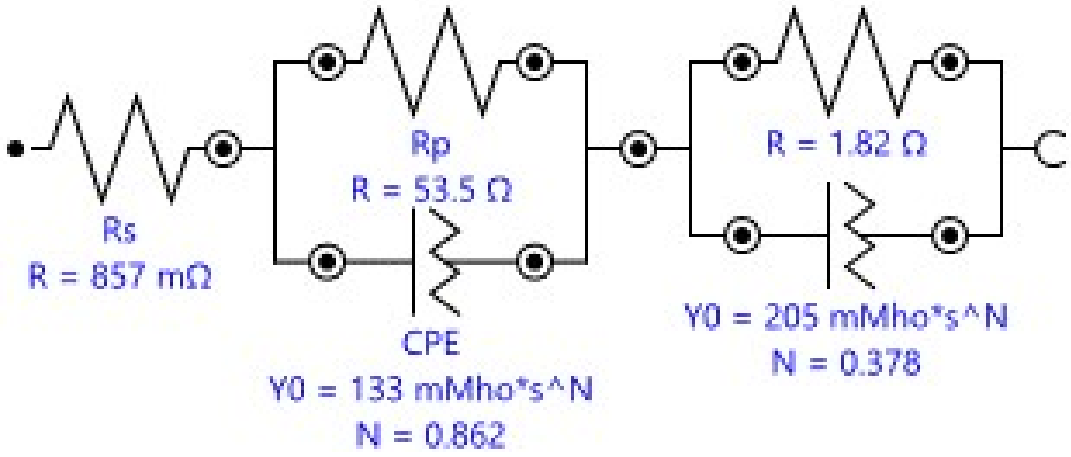

Fig. S22 Fitted Randles circuit for $CuFeS_2$.

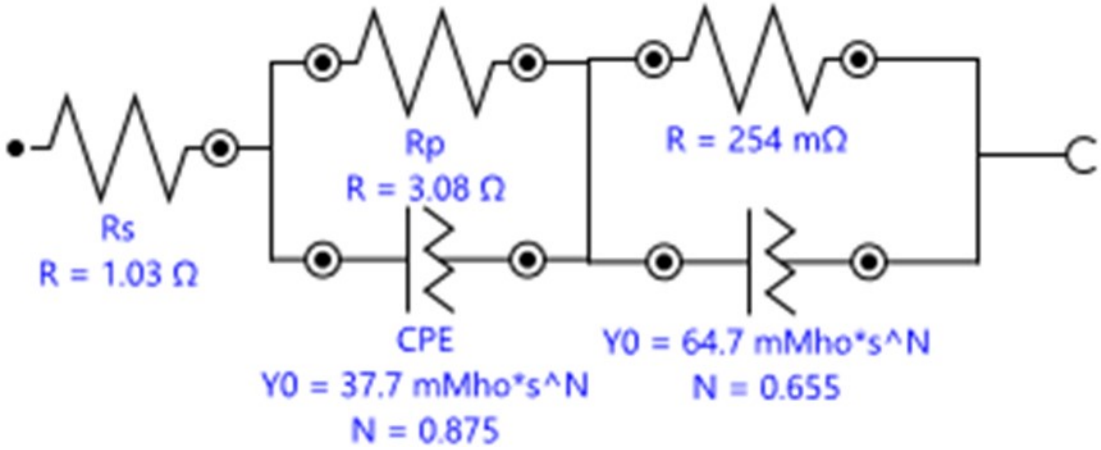

Fig. S23 Fitted Randles circuit for RuO_2.

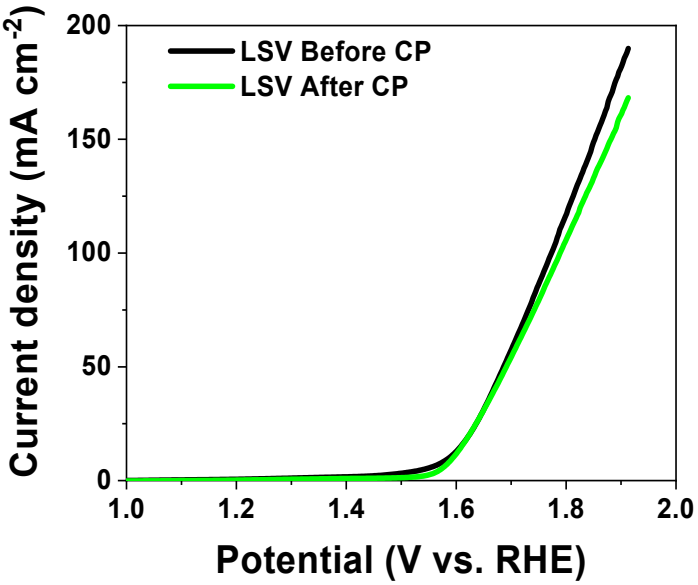

Fig. S24 LSV curves before and after long run chronoamperometry test of $CuFeS_2$ electrode.

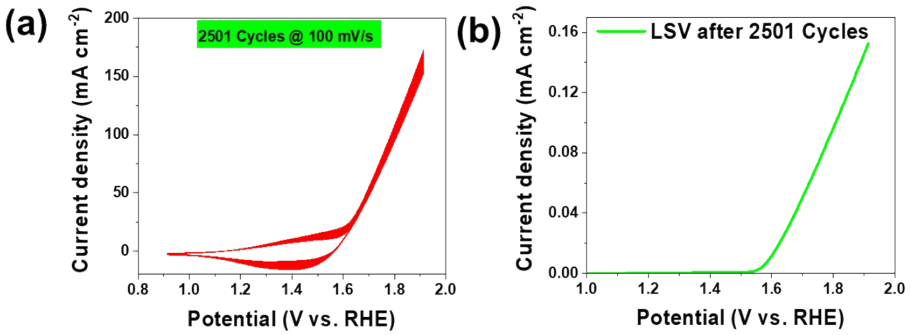

Fig. S25. (a) 2501 CV cycles recorded for the stability test and (b) LSV curves of the $CuFeS_2$ electrode after 2501 CV cycles.

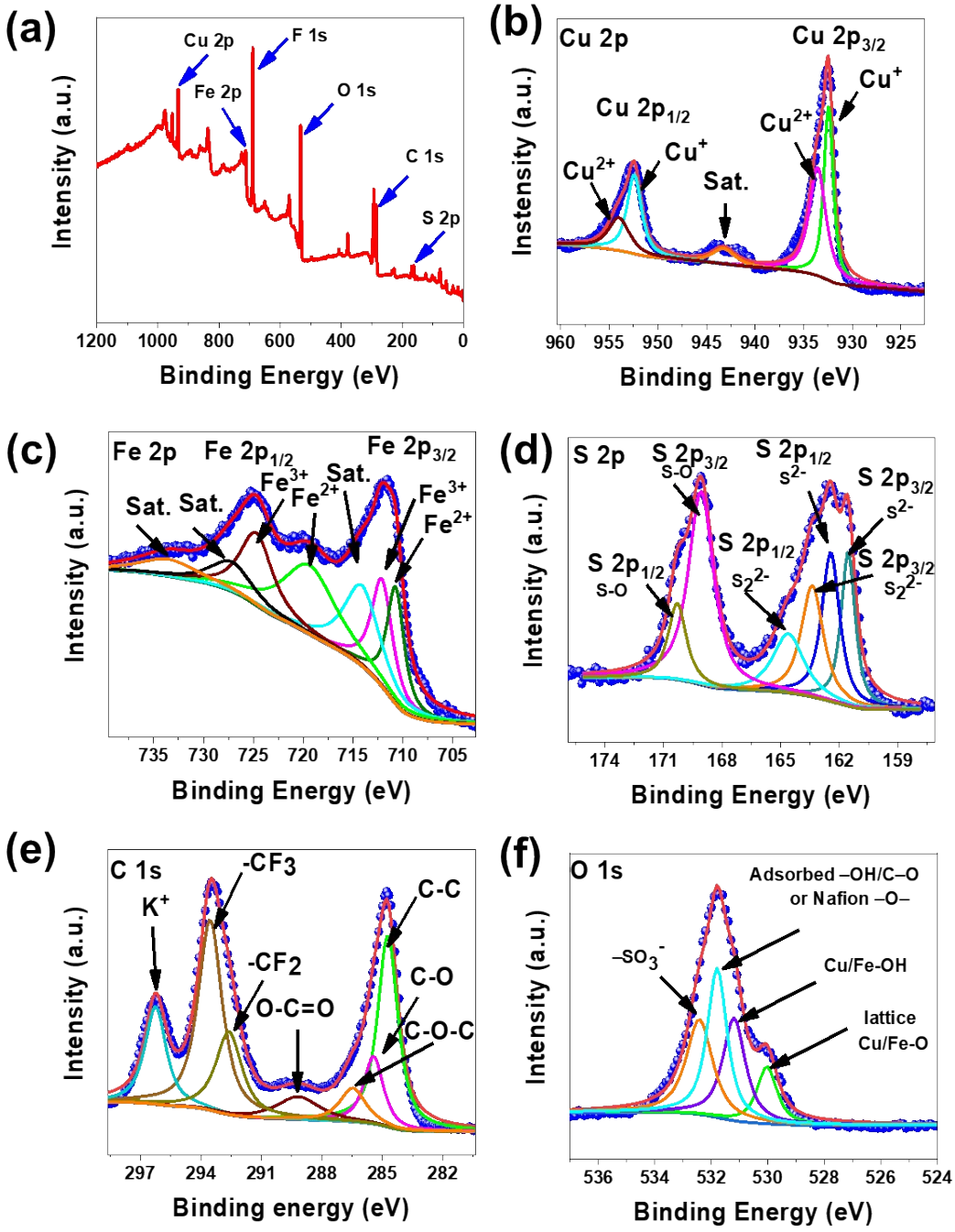

Fig. S26. XPS spectra of $CuFeS_2$ after the long-term chronopotentiometry (CP) test: (a) survey spectrum, and core-level spectra of (b) Cu 2p, (c) Fe 2p, (d) S 2p, (e) C 1s, and (f) O 1s.

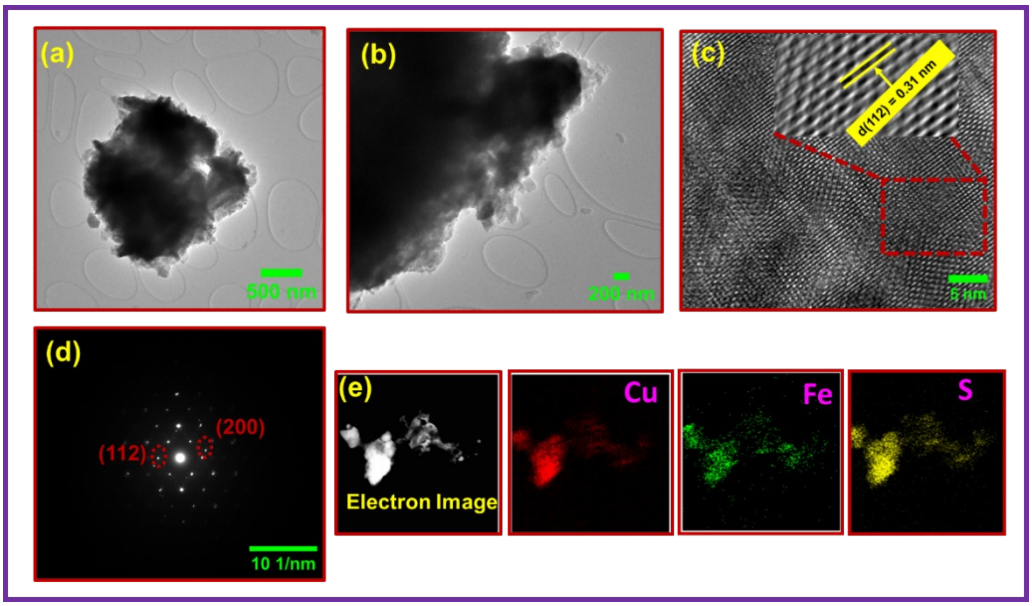

Fig. S27. (a, b) TEM micrographs, (c) HRTEM image with inset FFT pattern, (d) SAED pattern, and (e) EDS elemental mapping of Cu, Fe, and S for the $CuFeS_2$ electrode after the OER stability test.

Table S4. Comparison of OER performance with some other sulfide materials reported recently.

S. No.	Electrocatalysts	Electrolyte	Onset potential (mV) @10 mA cm^{-2}	Tafel slope (mV dec^{-1})	References
1	$FeCuS_2$/NG	1.0 M KOH	348.16	128.75	[6]
2	$CuFe(S_{0.8}Se_{0.2})_2$	1.0 M KOH	271	92.2	[7]
3	Fe-doped CuS/CuO/Copper Sheet	1.0 M KOH	340	31	[8]
4	CoMnNiS	1.0 M KOH	371	48	[9]
5	$Fe_{0.9}Co_{0.05}S_{1.05}$	1.0 M KOH	257	46	[10]
6	$NiCo_2S_4$/RGO	1.0 M KOH	366	65	[11]
7	$FeNiS_2$	1.0 M KOH	250	99	[12]
8	$CoFeS_2$/NC	1.0 M KOH	340	56.2	[13]
9	$CuCo_2S_4$/Carbon Cloth (CC)	1.0 M KOH	280	143	[14]
10	$CuFeS_2$	1.0 M KOH	356	148.7	This work.
11	RuO_2	1.0 M KOH	270	90	This work.

References:

1. V. Dimitrov and S. Sakka, *J. Appl. Phys.*, 1996, **79**, 1741-1745.
2. T. Moss, *Proc. Phys. Soc. Sec.* , 1950, **63**, 167.
3. N. Ravindra, S. Auluck and V. Srivastava, *Phys. Status Solidi B*, 1979, **93**, K155-K160.
4. P. Herve and L. Vandamme, *J. Appl. Phys.*, 1995, **77**, 5476-5477.
5. S. Tripathy, *Opt. Mater.*, 2015, **46**, 240-246.

6. G. Mayakrishnan, R. Vanaraj, J. Xiong, M. Farooq, A. Ullah, K. Zhang, S. C. Kim and I. S. Kim, *Energy Environ. Mater.*, 2024, **7**, e12788.

7. S. Huang, X. Cong, T. Ye, L. Liu, K. Peng, L. Zhang, J. Bao, P. Gao, Q. Chen and Q. He, *Inorg. Chem. Front.*, 2023, **10**, 2387-2398.

8. L. Tabassum, M. Khairul Islam, I. P. Perera, M. Li, X. Huang, H. Tasnim and S. L. Suib, *ACS Appl. Energy Mater.*, 2022, **5**, 12039-12048.

9. M. Verma, L. Sinha and P. M. Shirage, *J. Mater. Sci.: Mater. Electron.*, 2021, **32**, 12292-12307.

10. D. Zheng, Z. Jing, Q. Zhao, Y. Kim, P. Li, H. Xu, Z. Li and J. Lin, *Chem. Eng. J.*, 2020, **402**, 125069.

11. C. Shuai, Z. Mo, X. Niu, X. Yang, G. Liu, J. Wang, N. Liu and R. Guo, *J. Mater. Sci.*, 2020, **55**, 1627-1636.

12. N. Dalai and B. Jena, *ChemistrySelect*, 2023, **8**, e202204370.

13. J. Cai, H. Liu, Y. Luo, Y. Xiong, L. Zhang, S. Wang, K. Xiao and Z.-Q. Liu, *J. Energy Chem.*, 2022, **74**, 420-428.

14. C. Ren, Y. Chen, L. Du, Q. Wang, L. Li and G. Tian, *ChemElectroChem*, 2021, **8**, 1134-1140.